An Unconditionally Stable FDTD Method Using Tetrahedral Cells

Wilson A. Artuzi Jr.   —   Departamento de Engenharia Elétrica UFPR

Abstract— **The concept of the finite difference time domain method is applied to tetrahedral cells in order to permit its use with structures of complex shapes. Unconditional stability is achieved through the Newmark time discretization of wave equation and the conjugate gradient method with incomplete Cholesky preconditioning provides a fast solver for the system of linear equations to be evaluated every time step. Numerical experiments have shown that there exists an optimum time step value which conducts to an accurate solution with the minimum of two iterations per time step.**

Keywords— **FDTD, FETD, tetrahedral mesh, conjugate gradient**

I. INTRODUCTION

Time domain numerical solutions of Maxwell's equations have become powerful tools to predict phenomena and analyze devices involving electromagnetic wave propagation. Among them, the finite difference time domain (FDTD) method is of great importance [1].

The FDTD method, which is based on separate staggered orthogonal grids for the electric and magnetic field discretizations in space, has provided a robust second-order accurate algorithm for time domain electrodynamic computations and its use has been widely spread despite of the fact that arbitrary shaped structures do not match the orthogonal lattice. Several approaches have been developed in order to overcome this drawback. Some of them maintain the orthogonal grid basis [2]. Others are implemented on unstructured meshes but their use has not been continued because they can suffer from numerical instabilities depending upon the mesh being constructed [3],[4].

This work will show that the FDTD concept can be applied to tetrahedral meshes to obtain an unconditionally stable but implicit formulation which is more accurate but requires the solution of a linear system of equations every time step. The use of a preconditioned conjugate gradient solver, however, can provide a fast numerical processing reaching the minimum of two iterations per time step if a suitable time step duration is chosen. Accuracy issues are addressed through the evaluation of the resonant frequency of a metallic cylindrical cavity under different spatial and temporal sampling rates.

II. GEOMETRIC DEFINITIONS

The mathematical treatment of the problem will be focused on a tetrahedral cell at first and the formulation for the whole spatial domain will be achieved later by superposition. The combination of staggered elementary primary

W. A. Artuzi Jr. is with Department of Electrical Engineering, Parana Federal University, Curitiba , PR, Brasil, artuzi@eletrica.ufpr.br.
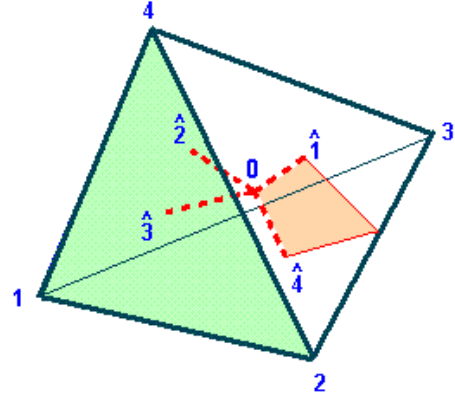

Fig. 1. A tetrahedral cell. Points 1, 2, 3 and 4 are referred to the primary mesh element (solid lines) and points 0, $\hat{1}$, $\hat{2}$, $\hat{3}$ and $\hat{4}$ are referred to the secondary one (dotted lines). Highlighted surfaces indicate the primary face 3 and the secondary face 23.

and secondary mesh elements comprising a region of homogeneous medium will be called a cell, as shown in Fig.1.

The primary mesh element is formed by points 1, 2, 3 and 4 whose coordinates are provided as the output of mesh generators. Connection of two points by a straight line form a primary edge to be denoted by two indices in reference to these points and its length vector is obtained by

$$\vec{L}_{pq} = \vec{R}_p - \vec{R}_q \qquad (1)$$

where $\vec{R}_p$ and $\vec{R}_q$ are position vectors of vertices p and q. These vectors can be arranged into the primary length matrix as

$$\mathbf{L} = \begin{bmatrix} L_{12x} & L_{12y} & L_{12z} \\ L_{13x} & L_{13y} & L_{13z} \\ L_{14x} & L_{14y} & L_{14z} \\ L_{23x} & L_{23y} & L_{23z} \\ L_{24x} & L_{24y} & L_{24z} \\ L_{34x} & L_{34y} & L_{34z} \end{bmatrix} \qquad (2)$$

Three edges form a primary triangular face to be denoted by one index in reference to the point excluded from this face. The area vector of a primary face, pointing outward the cell, is

$$\vec{S}_s = \frac{(-1)^s}{2} \ \vec{L}_{pq} \times \vec{L}_{qr} \qquad (3)$$

where p, q, r and s stand for cyclic permutations of indices 1, 2, 3 and 4. These can be arranged into the primary area

matrix as

$$\mathbf{S} = \begin{bmatrix} S_{1x} & S_{1y} & S_{1z} \\ S_{2x} & S_{2y} & S_{2z} \\ S_{3x} & S_{3y} & S_{3z} \\ S_{4x} & S_{4y} & S_{4z} \end{bmatrix} \tag{4}$$

The secondary mesh element consists of a point 0 which is the barycenter of the cell and one point on each face $\hat{1}$, $\hat{2}$, $\hat{3}$ and $\hat{4}$ which are their barycenters. Connection of point 0 with the barycenter of a face by a straight line form a secondary edge whose index indicates the correspondence with this barycenter and its length vector is

$$\vec{L}_s = \frac{\vec{L}_{ps} + \vec{L}_{qs} + \vec{L}_{rs}}{12} \tag{5}$$

and they form the secondary length matrix as

$$\hat{\mathbf{L}} = \begin{bmatrix} L_{1x} & L_{1x} & L_{1x} \\ L_{2x} & L_{2x} & L_{2x} \\ L_{3x} & L_{3x} & L_{3z} \\ L_{4x} & L_{4y} & L_{4z} \end{bmatrix} \tag{6}$$

Two secondary edges define a secondary face whose indices correspond to the points excluded from this face and its area vector is

$$\vec{S}_{pq} = \frac{\vec{S}_p - \vec{S}_q}{12} \tag{7}$$

which form the secondary area matrix

$$\hat{\mathbf{S}} = \begin{bmatrix} S_{12x} & S_{12y} & S_{12z} \\ S_{13x} & S_{13y} & S_{13z} \\ S_{14x} & S_{14y} & S_{14z} \\ S_{23x} & S_{23y} & S_{23z} \\ S_{24x} & S_{24y} & S_{24z} \\ S_{34x} & S_{34y} & S_{34z} \end{bmatrix} \tag{8}$$

These length and area matrices will be useful in the spatial discretization of Maxwell's equations to be explained in the next section.

III. Matrix Wave Equation

As in finite element methods [5], matrix equations have shown to yield compact notation and allow for direct implementation in computational algorithms therefore they will be used here instead of the notation commonly encountered in FDTD formulations. The matrix wave equation will be derived from the Maxwell's equations in integral forms

$$\oint_L \vec{e}.d\vec{L} = -\frac{\partial}{\partial t}\int_S \vec{b}.d\vec{S} \tag{9}$$

$$\oint_L \vec{h}.d\vec{L} = \frac{\partial}{\partial t}\int_S \vec{d}.d\vec{S} + \int_S \vec{j}.d\vec{S} \tag{10}$$

$$\oint_S \vec{d}.d\vec{S} = \int_V \rho \, dV \tag{11}$$

$$\oint_S \vec{b}.d\vec{S} = 0 \tag{12}$$

being $\vec{e}$ and $\vec{h}$ the electric and magnetic field intensities, $\vec{d}$ and $\vec{b}$ the electric and magnetic flux densities, ρ and $\vec{j}$ the electric charge and current densities, respectively.

Here, the spatial discretization will be based on a piecewise constant approximation of the electromagnetic quantities, i.e., they will be assumed to be constant inside a cell and therefore (11) and (12) are automatically satisfied once no charge accumulation is being considered.

The application of (9) on each primary triangular face gives

$$\mathbf{\Sigma} \, \mathbf{L} \, \mathbf{e} = -\frac{\partial}{\partial t}\mathbf{S} \, \mathbf{b} \tag{13}$$

where the small bold letters represent the time dependent vectors inside the cell

$$\mathbf{e} = \begin{bmatrix} e_x & e_y & e_z \end{bmatrix}^T \tag{14}$$

$$\mathbf{b} = \begin{bmatrix} b_x & b_y & b_z \end{bmatrix}^T \tag{15}$$

and the capital and greek bold letters represent time invariant matrices. The matrix

$$\mathbf{\Sigma} = \begin{bmatrix} 0 & 0 & 0 & -1 & 1 & -1 \\ 0 & 1 & -1 & 0 & 0 & 1 \\ -1 & 0 & 1 & 0 & -1 & 0 \\ 1 & -1 & 0 & 1 & 0 & 0 \end{bmatrix} \tag{16}$$

completes the circulation around each triangular face through proper summation of the line integrals along the edges.

The application of (10) on each secondary face gives

$$\mathbf{\Sigma}^T \, \hat{\mathbf{L}} \, \boldsymbol{\nu} \, \mathbf{b} = \frac{\partial}{\partial t}\hat{\mathbf{S}} \, \boldsymbol{\varepsilon} \, \mathbf{e} + \hat{\mathbf{S}} \, \boldsymbol{\sigma} \, \mathbf{e} + \hat{\mathbf{S}} \, \mathbf{j} \tag{17}$$

where $\boldsymbol{\nu}$, $\boldsymbol{\varepsilon}$ and $\boldsymbol{\sigma}$ are the magnetic reluctivity (inverse of magnetic permeability), electric permittivity and electric conductivity tensors, respectively, and

$$\mathbf{j} = \begin{bmatrix} j_x & j_y & j_z \end{bmatrix}^T \tag{18}$$

is the excitation current density vector.

The matrix curl equations (13) and (17) can be combined and cast as a matrix wave equation of the form

$$\mathbf{C}\frac{d}{dt}\mathbf{v} + \mathbf{G} \, \mathbf{v} + \mathbf{K} \int_0^t \mathbf{v} \, dt = \mathbf{i} \tag{19}$$

where

$$\mathbf{i} = \hat{\mathbf{S}}\mathbf{j} \quad \text{and} \quad \mathbf{v} = -\mathbf{L}\,\mathbf{e} \tag{20}$$

are the excitation current and the unknown voltage vectors along the primary edges and

$$\mathbf{C} = \hat{\mathbf{S}} \, \boldsymbol{\varepsilon} \, (\mathbf{L}^T\mathbf{L})^{-1}\mathbf{L}^T \tag{21}$$

$$\mathbf{G} = \hat{\mathbf{S}} \, \boldsymbol{\sigma} \, (\mathbf{L}^T\mathbf{L})^{-1}\mathbf{L}^T \tag{22}$$

$$\mathbf{K} = \mathbf{\Sigma}^T \, \hat{\mathbf{L}} \, \boldsymbol{\nu} \, (\mathbf{S}^T\mathbf{S})^{-1}\mathbf{S}^T \, \mathbf{\Sigma} \tag{23}$$

are the capacitance, conductance and reluctance matrices of a cell, respectively. Because $\mathbf{L}$ and $\mathbf{S}$ are not square matrices their inverse cannot be found. A least squares solution, however, can be attained by applying the Moore-Penrose generalized inversion. The global wave equation is achieved by performing the superposition of elements of $\mathbf{C}$, $\mathbf{G}$ and $\mathbf{K}$ when the edges are addressed under a global numbering procedure [5].

IV. Time Stepping Solution

Once the global matrix equation has been obtained, it must be solved for the time dependent voltages $\mathbf{v}$ as a response to the excitation currents $\mathbf{i}$. The FDTD method employs the central difference approximation for the time derivatives to arrive at a conditionally stable time stepping solution. Stability is limited to a maximum constraint of the time step duration which is roughly proportional to the dimensions of the smallest cell [1]. The same method could be used here as well, but the Newmark method [6],[7] is more convenient since it leads to a stable solution regardless of the time step duration. This method is not usual in FDTD algorithms because it conducts to an implicit solution, i.e., a system of linear equations has to be solved every step, but it is advantageous in the present formulation as the implicit solution arrises anyway.

To apply the Newmark method, the global wave equation is rewritten as

$$\mathbf{C}\frac{d^2}{dt^2}\mathbf{w} + \mathbf{G}\frac{d}{dt}\mathbf{w} + \mathbf{K}\,\mathbf{w} = \mathbf{i} \qquad (24)$$

with

$$\mathbf{w} = \int_0^t \mathbf{v}\ dt$$

The time discretization is attained by using central differences and a weighted average as

$$\mathbf{C}\frac{\mathbf{w_{n+1}} - 2\mathbf{w_n} + \mathbf{w_{n-1}}}{\Delta t^2} + \mathbf{G}\frac{\mathbf{w_{n+1}} - \mathbf{w_{n-1}}}{2\Delta t} +$$
$$+ \mathbf{K}\frac{\mathbf{w_{n+1}} + 2\mathbf{w_n} + \mathbf{w_{n-1}}}{4} = \mathbf{i_n} \quad (25)$$

where Δt is the time step duration and the index n represents the time instant $t = n\Delta t$. The difference equation (25) can be rearranged as the following set of recursive equations

$$(\mathbf{C} + \frac{\Delta t}{2}\mathbf{G} + \frac{\Delta t^2}{4}\mathbf{K})\,\mathbf{u_{n+1}} = \mathbf{i_n} - \mathbf{G}\,\mathbf{v_n} - \mathbf{K}\,\mathbf{w_n} \quad (26)$$

$$\mathbf{v_{n+1}} = \mathbf{v_n} + \Delta t\,\mathbf{u_{n+1}} \qquad (27)$$

$$\mathbf{w_{n+1}} = \mathbf{w_n} + \Delta t\,\mathbf{v_{n+1}} \qquad (28)$$

Since $\mathbf{C}$, $\mathbf{G}$ and $\mathbf{K}$ are real and symmetric sparse matrices with positive elements on the main diagonal, the conjugate gradient method with incomplete Cholesky preconditioning (ICCG) [8] is one of the most appropriate solvers to find $\mathbf{u_{n+1}}$ in (26) taking a null vector as initial guess. The desired voltage vector $\mathbf{v_{n+1}}$ appears in (27). Convergence aspects related to the number of ICCG iterations will be discussed in the next section by means of numerical experiments.

V. Numerical Experiments

Testing of the proposed formulation is implemented by computing the resonant frequency of a lossless metallic cylindrical cavity under different spatial and temporal sampling densities. The cavity is filled with air and it has a diameter of 380mm and a height of 300mm. The dependence of the accuracy on time and space discretizations will be investigated separately. The investigation will be based on three parameters: the number of ICCG iterations and the average temporal and spatial sampling densities to be defined by

$$\xi = \frac{L_{av}}{c\Delta t} \qquad (29)$$

$$\eta = \frac{\lambda_0}{L_{av}} \qquad (30)$$

respectively, where c is the velocity of light, λ_0 is the free space wavelength at the resonant frequency and L_{av} is the average of all primary edge lengths.

A. Modeling

The perfect electric conductor boundaries are modelled by imposing null voltages on the edges that lay on them. A current source is impressed along the cavity axis in order to excite the fundamental TM_{010} mode. The source shape in time is a Gaussian derivative pulse having a width of 1.7ns to span significant field amplitudes near the resonant frequency. Voltage samples are taken along the cavity axis during 50ns and are Fourier transformed to identify the resonant frequency value.

B. Temporal Sampling

In order to verify the accuracy behavior against the discretization in time, a mesh having average spatial sampling density of $\eta = 15$ is implemented. The relative errors of the resonant frequency are plotted with circle marks, in Fig.2, for temporal sampling densities ranging from 1 to 10. The corresponding maximum relative residuals of the ICCG are plotted together with square marks. The ICCG algorithm is run for 2 (dotted lines), 3 (dashed lines) and 4 (solid lines) iterations per time step. It can be observed
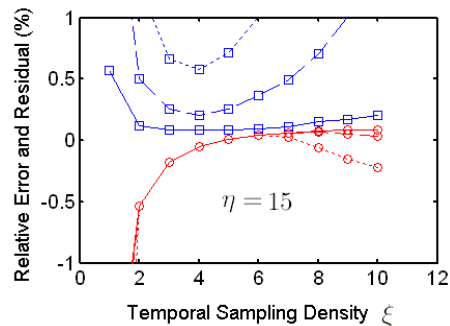

Fig. 2. Relative error of resonant frequency ($\bigcirc$) and relative residual of ICCG ($\square$) against the average temporal sampling density. ICCG algorihm is run for 2 ($\cdots$), 3 (- - -) and 4 (—) iterations per time step.

that the relative error does not change significantly with the number of ICCG iterations in the range $2 \leq \xi \leq 6$. This means that a minimum of 2 iterations per time step can be used within this range and increasing the number of iterations does not affect the solution at all, although the

relative residual decreases. For $\xi < 2$, the absolute value of the relative error increases drastically, but the solution maintains stable. For $\xi > 6$, the relative error reaches a plateau, but more ICCG iterations are required as ξ increases. All curves of relative residual have a minimum at $\xi = 4$, giving the insight that close to this temporal sampling density the best ICCG convergence is reached. For comparison, the maximum temporal sampling density allowed for a stable FDTD solution with cubic cells is $\xi = \sqrt{3}$ (inverse of numerical stability factor).

C. Spatial Sampling

Maintaining the optimum temporal sampling density of $\xi = 4$ and two ICCG iterations per time step, the accuracy has been investigated against the spatial sampling density as shown in Fig.3 with square marks. A reference line is plotted to show the second-order convergence of the method.
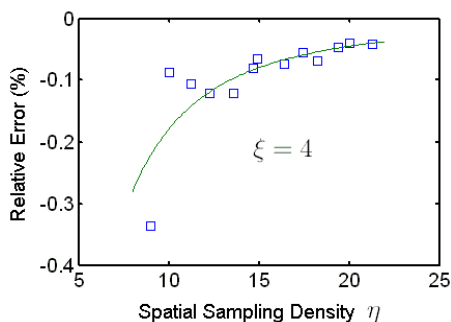

Fig. 3. Relative error of resonant frequency against the spatial sampling density ($\square$). The solid line represents a second-order accuracy reference.

D. Discussion

It is a well known fact that increasing the time step duration degrades the accuracy of the Newmark technique, thus making use of very large time steps is not recommendable though the solution is stable [6]. On the other hand, it is interesting to notice that reducing the time step duration degrades the ICCG convergence. This can be explained as the condition number of the matrix on the left-hand side of (26) is increased for small time steps since matrix K is indefinite [7]. The optimum temporal sampling density $\xi = 4$ appears to be the best compromise between both situations.

Results obtained with orthogonal grid FDTD simulations [2] are used for comparison. In these simulations, the cavity is tilted with respect to the grid axes and the maximum errors are summarized in Table I for spatial sampling densities of $\eta = 10$ and $\eta = 20$. The staircase approach leads to the highest errors while the contour-path and the Dey-Mittra approaches reach better results for refined meshes. The present method provides the best accuracy even for the lowest spatial sampling density. This represents a great advantage which makes this method competitive despite of its implicit nature. Unfortunately, CPU

time and memory requirements are not available in [2] for comparison.

TABLE I

RELATIVE ERRORS FOR RESONANT FREQUENCY OF CYLINDRICAL CAVITY UNDER DIFFERENT FDTD IMPLEMENTATIONS

Absolute Percentual Error		
η	10	20
Staircase [2]	5.3	2.4
Contour-Path [2]	2.2	1.4
Dey-Mittra [2]	2.9	0.4
This Method ($\xi = 4$)	0.1	0.05

Finite element time domain methods using first order edge basis functions produce errors similar to those obtained by this method [6]. Furthermore, the low frequency spurious response reported in [7] was not noticed. This may be due to the use of $\mathbf{w}$ instead of $\mathbf{v}$ in the Newmark formulation. Since $\mathbf{v}$ is the time derivative of $\mathbf{w}$, a slow spurious response in $\mathbf{w}$ would have negligible effect in $\mathbf{v}$.

VI. CONCLUSION

An unconditionally stable time domain formulation for electrodynamic computations using tetrahedral meshes has been presented. The method is more accurate than FDTD implementations with orthogonal grids for modeling curved surfaces. Its implicit nature is overcome through the incomplete Cholesky preconditioned conjugate gradient solver and two iterations per time step can be achieved when the optimum time step duration is used. Finally, an empirical formula for estimating this optimum value has been presented.

REFERENCES

[1] A. Taflove, *Computational Electrodynamics: The Finite-Difference Time-Domain Method*, Artech House, Boston, 1995.
[2] C. J. Railton and J. B. Schneider, "An analytical and numerical analysis of several locally conformal FDTD schemes," *IEEE Transactions on Microwave Theory and Tech.*, vol.47, pp.56-66, Jan. 1999.
[3] N. K. Madsen, "Divergence preserving discrete surface integral methods for Maxwell's curl equations using non-orthogonal unstructured grids, " *Journal of Computational Physics*, vol.119, pp.34-45, 1995.
[4] S. D. Gedney, F. S. Lansing and D. L. Rascoe, "Full wave analysis of microwave monolithic circuit devices using a generalized yee-algorithm based on unstructured grid, " *IEEE Trans. Microwave Theory and Tech.*, vol.44, pp.1393-1400, Aug. 1996.
[5] M. N. O. Sadiku, *Elements of Electromagnetics*, Oxford University Press, 3rd ed., 2000.
[6] S. D. Gedney and U. Navsariwala, "An unconditionally stable finite element time-domain solution of the vector wave equation, " *IEEE Microwave and Guided Wave Lett.*, vol.5, pp.332-334, Oct. 1995.
[7] D. K. Sun, J. F. Lee and Z. Cendes, "The transfinite-element time-domain method," *IEEE Trans. Microwave Theory and Tech.*, vol.51, pp.2097-2105, Oct. 2003.
[8] G. Kuo-Petravic and M. Petravic,"A program generator for the incomplete cholesky conjugate gradient (ICCG) method with a symmetrizing preprocessor," *Computer Physics Communications*, Vol.22, pp.33-48, Feb.Mar. 1981.